[Research Paper] 대한금속·재료학회지 (*Korean J. Met. Mater.*), Vol. 56, No. 7 (2018) pp.544-550
DOI: 10.3365/KJMM.2018.56.7.544

Charge Transport and Thermoelectric Properties of N-type $Bi_{2-x}Sb_xTe_{3-y}Se_y:I_m$ Prepared by Encapsulated Melting and Hot Pressing

Woo-Jin Jung, Hyeok-Jin Kim, and Il-Ho Kim*

Department of Materials Science and Engineering, Korea National University of Transportation, Chungju 27469, Republic of Korea

Abstract: Iodine-doped n-type $Bi_{2-x}Sb_xTe_{3-y}Se_y:I_m$ ($x = 0.1–0.2$, $y = 0.15–0.6$, and $m = 0.0025–0.005$) quaternary solid solutions were prepared by encapsulated melting (EM) and hot pressing (HP). The lattice constants of the resulting materials decreased with increasing Sb and Se contents, whereas the amount of I dopant was too small to significantly affect the lattice constants. An average relative density of 97% was obtained for the hot-pressed specimens. All specimens indicated n-type conductions in the temperature range of 323 to 523 K, and the electrical conductivity decreased with increasing temperature, exhibiting the typical characteristics of degenerate semiconductors. The electrical conductivity and the thermal conductivity decreased with increasing Se content, whereas they increased with I doping. This was a result of changes in the carrier concentrations due to Se substitution and I doping, and from the decreased lattice thermal conductivity due to increased alloy scattering. However, the changes in electrical and thermal conductivity caused by Sb substitution were not significant. The maximum figure of merit, ZT_{max}, of 0.84, was achieved at 473 K for $Bi_{1.9}Sb_{0.1}Te_{2.85}Se_{0.15}:I_{0.0025}$.

(Received May 9, 2018; Accepted June 1, 2018)

Keywords: thermoelectric, bismuth telluride, charge transport, mechanical alloying, hot pressing

1. INTRODUCTION

Thermoelectric energy conversion has attracted considerable attention for use in various power generation applications that use waste heat and solid-state electronic cooling [1,2]. The thermoelectric performance of a material is typically expressed by the dimensionless figure of merit (ZT),

$$ZT = \frac{\alpha^2 \sigma T}{\kappa} \quad (1)$$

where α is the Seebeck coefficient, σ is the electrical conductivity, κ is the thermal conductivity, and T is the absolute temperature [3]. High-performance thermoelectric materials require a high Seebeck coefficient and electrical conductivity and a low thermal conductivity. These three parameters depend mainly on carrier concentration and temperature.

Bi_2Te_3 has a rhombohedral $R\bar{3}m$ crystal structure, and Bi_2Te_3-based compounds have excellent thermoelectric properties at room temperature [4]. For n-type $Bi_2(Te,Se)_3$, the Bi_2Te_3-Bi_2Se_3 forms a solid solution of $Bi_2Te_{3-y}Se_y$ because the two crystals have identical crystal structures and similar electronic structures. The Se atom can occupy the Te site, increasing alloy scattering caused by phonons and electrons, thereby resulting in a reduction in lattice thermal conductivity and carrier mobility [5,6]. However, because the carrier concentration is decreased, donor doping is necessary to supply additional electrons. The semiconducting behavior of Bi_2Te_3-based alloys can be tuned by doping [7], and group 7 elements such as Cl, Br, and I can optimize the carrier concentration of n-type $Bi_2Te_{3-y}Se_y$. However, these elements are unstable at high vapor pressures at elevated temperatures and cannot be used alone as dopants. Instead, compound dopants such as SbI_3 and $CdCl_2$ can be used [8-10]. The effect of Se on n-type Bi_2Te_3-based materials has been extensively studied, but the effects of Sb and Se on the quaternary

*Corresponding Author: Il-Ho Kim
[Tel: +82-43-841-5387, E-mail: ihkim@ut.ac.kr]

Bi–Sb–Te–Se systems are not well-known. Fan et al. [11] reported a ZT of 0.66 at 343 K for ternary n-type $Bi_2Te_{2.85}Se_{0.15}$ prepared by mechanical alloying and equal channel angular extrusion. Wang et al. [12] reported a ZT of 1.0 at 460 K for quaternary n-type $Bi_{1.9}Sb_{0.1}Te_{2.55}Se_{0.45}$ prepared by melt spinning and spark plasma sintering. In this study, I-doped quaternary n-type $Bi_{2-x}Sb_xTe_{3-y}Se_y:I_m$ solid solutions were prepared by encapsulated melting (EM) and hot pressing (HP), and the effects of the Sb and Se substitutions as well as I doping on the change transport and the thermoelectric properties of the fabricated material were examined.

2. EXPERIMENTAL PROCEDURE

$Bi_{2-x}Sb_xTe_{3-y}Se_y:I_m$ ($x = 0.1–0.2$, $y = 0.15–0.6$, and $m = 0.0025–0.005$) solid solutions were synthesized using EM. Bi (purity 99.999%, 5N Plus), Sb (purity 99.999%, 5N Plus), Te (purity 99.999%, 5N Plus), Se (purity 99.999%, ASARCO), and SbI_3 (purity 99.9%, Kojundo) were weighed according to the desired stoichiometry and loaded into a quartz ampoule. The sealed quartz ampoule was heated at 1073 K for 4 h, and the ingot was crushed into powder with particle sizes less than 75 μm. The synthesized powders were sintered using HP in a cylindrical graphite die (internal diameter of 10 mm) at 723 K under a pressure of 70 MPa for 1 h in a vacuum. The phases and lattice constants of the hot-pressed specimens were analyzed by X-ray diffraction (XRD; Bruker D8-Advance) with Cu Kα radiation, and the diffraction patterns were measured in the θ-2θ mode (2θ of 10–90°) at a scan speed of 0.4 s/step and a step size of 0.02°. The fractured surfaces and elemental distributions of the specimens were analyzed via scanning electron microscopy (SEM; FEI Quanta 400) equipped with an energy-dispersive spectrometer (EDS; JSM-7000F).

The Hall coefficient, carrier concentration, and mobility were measured using the van der Pauw method (Keithley 7065) with a magnetic field of 1 T and electric current of 50 mA at room temperature. The Seebeck coefficient and electrical conductivity were measured using the temperature differential and DC 4-probe methods (Ulvac-Riko ZEM-3) in a He atmosphere. The thermal conductivity was calculated from the specific heat, density, and thermal diffusivity measured by the laser flash method (Ulvac-Riko, TC-9000H). The power factor and the dimensionless figure of merit were evaluated at temperatures ranging from 323 to 523 K.

3. RESULTS AND DISCUSSION

Figure 1 shows the XRD patterns of the $Bi_{2-x}Sb_xTe_{3-y}Se_y:I_m$ solid solutions. As shown in Fig. 1(a), all of the diffraction peaks corresponded to the standard diffraction data (ICDD PDF# 15-0863), which

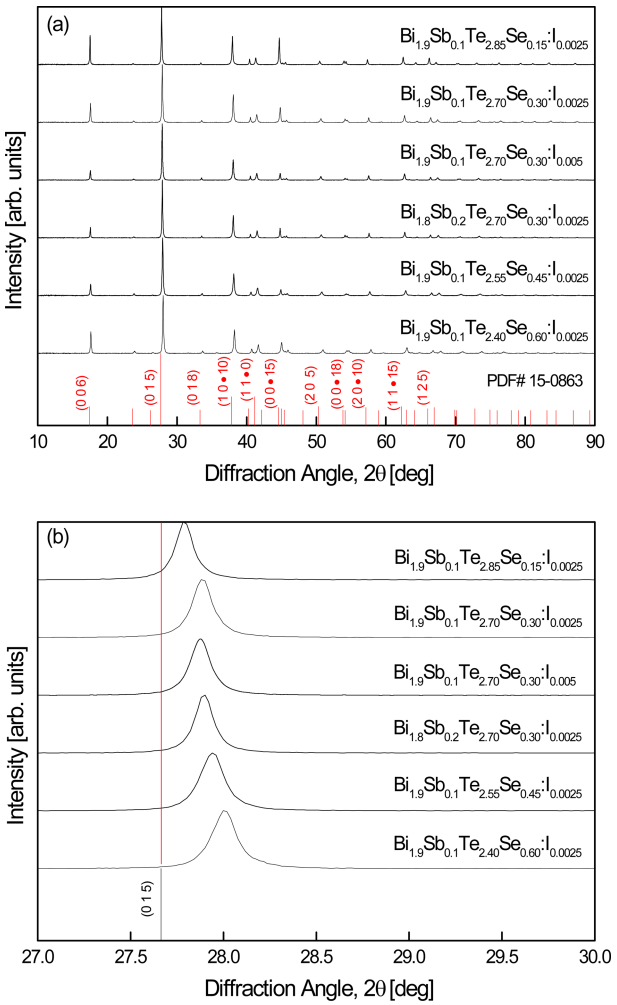

Fig. 1. (a) XRD patterns of $Bi_{2-x}Sb_xTe_{3-y}Se_y:I_m$ solid solutions and (b) diffraction peak shifts due to Se substitutions.

Table 1. Chemical compositions, lattice constants, relative densities, and charge transport properties of $Bi_{2-x}Sb_xTe_{3-y}Se_y:I_m$ at room temperature.

Specimen		Lattice Constant [nm]		Relative Density [%]	Hall Coefficient [cm^3C^{-1}]	Mobility [$cm^2V^{-1}s^{-1}$]	Carrier Concentration [cm^{-3}]	Effective Mass [m^*/m_0]
Designation	Actual Composition	a	c					
$Bi_{1.9}Sb_{0.1}Te_{2.85}Se_{0.15}:I_{0.0025}$	$Bi_{1.91}Sb_{0.1}Te_{2.83}Se_{0.16}I_{0.0025}$	0.4366	3.0371	97.4	-0.0472	89.2	1.3×10^{20}	1.38
$Bi_{1.9}Sb_{0.1}Te_{2.70}Se_{0.30}:I_{0.0025}$	$Bi_{1.92}Sb_{0.1}Te_{2.67}Se_{0.31}I_{0.0025}$	0.4346	3.0325	98.2	-0.0726	123.5	8.6×10^{19}	1.00
$Bi_{1.9}Sb_{0.1}Te_{2.70}Se_{0.30}:I_{0.005}$	$Bi_{1.89}Sb_{0.1}Te_{2.69}Se_{0.32}I_{0.005}$	0.4349	3.0337	98.3	-0.0374	79.6	1.7×10^{20}	1.35
$Bi_{1.8}Sb_{0.2}Te_{2.70}Se_{0.30}:I_{0.0025}$	$Bi_{1.81}Sb_{0.19}Te_{2.69}Se_{0.31}I_{0.0025}$	0.4345	3.0296	95.4	-0.0650	112.7	9.6×10^{19}	1.09
$Bi_{1.9}Sb_{0.1}Te_{2.55}Se_{0.45}:I_{0.0025}$	$Bi_{1.92}Sb_{0.1}Te_{2.54}Se_{0.46}I_{0.0025}$	0.4338	3.0257	96.2	-0.0757	123.1	8.3×10^{19}	1.02
$Bi_{1.9}Sb_{0.1}Te_{2.40}Se_{0.60}:I_{0.0025}$	$Bi_{1.89}Sb_{0.1}Te_{2.40}Se_{0.61}I_{0.0025}$	0.4327	3.0199	97.4	-0.0811	92.6	7.7×10^{19}	1.03

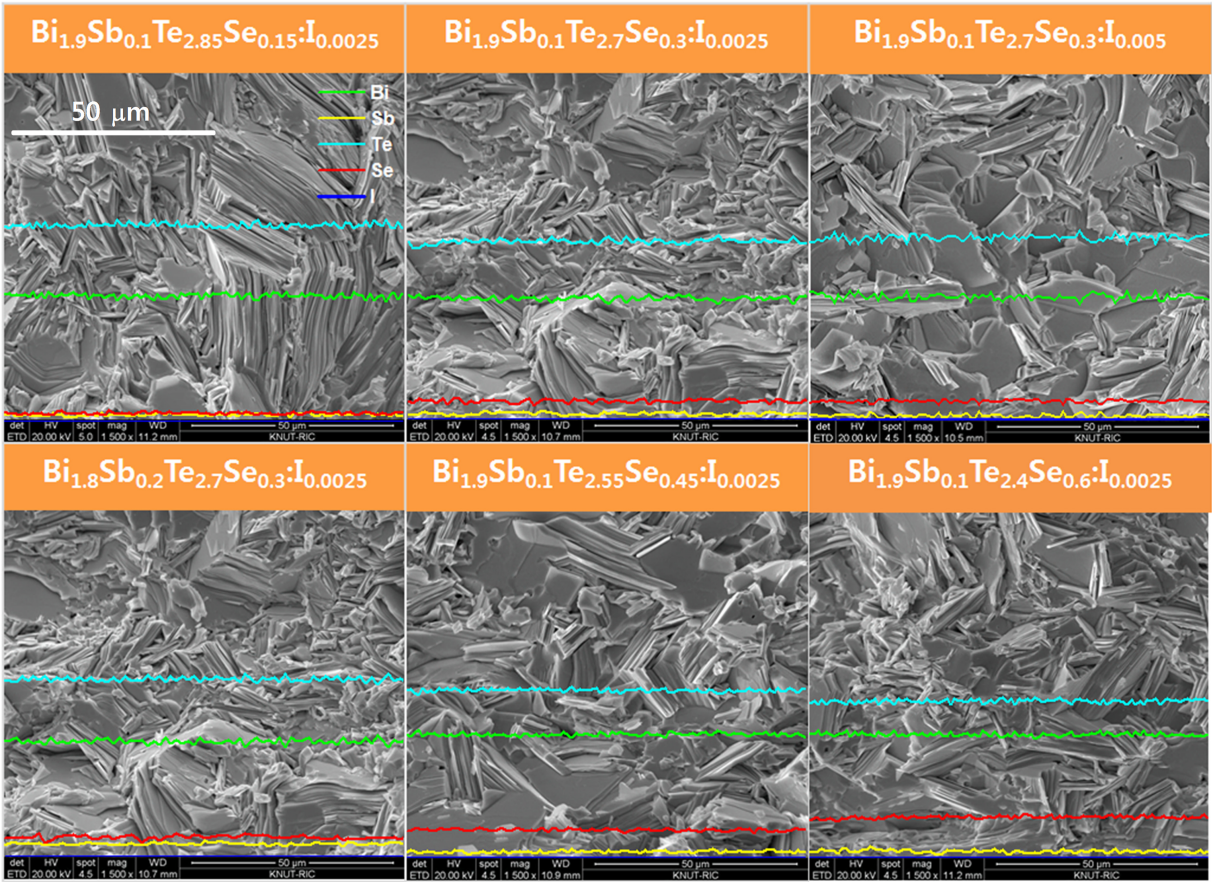

Fig. 2. SEM images of the fractured surfaces and elemental distributions of $Bi_{2-x}Sb_xTe_{3-y}Se_y:I_m$.

indicated that quaternary $Bi_{2-x}Sb_xTe_{3-y}Se_y$ solid solutions had been successfully synthesized. No secondary phases were observed, and the doping amount of I was so small that it could not be detected in the XRD patterns. Figure 1(b) shows the enlarged diffraction peaks of the (015) planes, which confirm the peak shift to higher angles with increasing Sb and Se contents. Table 1 lists the chemical compositions, lattice constants, and relative densities of the prepared $Bi_{2-x}Sb_xTe_{3-y}Se_y:I_m$ samples. The lattice constants decreased with increasing Sb and Se content because of the smaller atomic radii of Sb (0.145 nm) and Se (0.115 nm) compared with those of Bi (0.160 nm) and Te (0.140 nm) [13,14]. These results confirmed the

substitutions of Sb for Bi and Se for Te. The lattice constants were largely unaffected by the I dopant content. The relative densities of the HP specimens were higher than 97% on an average.

Figure 2 shows the SEM images of the fractured surface and elemental distribution of the hot-pressed $Bi_{2-x}Sb_xTe_{3-y}Se_y:I_m$. All component elements were distributed homogeneously, and plate-like particles were arranged randomly without preferred orientations. The microstructure was largely unchanged by Sb/Bi and Se/Te substitutions as well as I doping.

The charge transport properties of $Bi_{2-x}Sb_xTe_{3-y}Se_y:I_m$ at room temperature are listed in Table 1. All specimens had negative Hall coefficients, indicating n-type conductions, and the carrier concentration decreased with increasing Se content. The carrier concentration increased and mobility decreased with increasing Sb substitution and I doping. Anion vacancies and antisite defects in Bi_2Te_3-based materials strongly influence their charge transport properties [15,16]. In Bi_2Te_3, when $\gamma < 3/2$ (γ: the ratio of anionic to cationic components), excess Bi atoms occupy the Te sites to generate Bi_{Te} antisite defects, which act as electron acceptors [17]:

$$Bi_{Bi} + V_{Te}^{\bullet\bullet} + 2e' \rightarrow V_{Bi}^{\prime\prime\prime} + Bi'_{Te} + 4h^{\bullet} \quad (2)$$

However, when $\gamma > 3/2$, excess Te atoms occupy the Bi sites to generate Te_{Bi} antisite defects, which act as electron donors [18]:

$$Te_{Te} + V_{Bi}^{\prime\prime\prime} + 3h^{\bullet} \rightarrow V_{Te}^{\bullet\bullet} + Te_{Bi}^{\bullet} + 3e' \quad (3)$$

The effective masses of the carriers were larger than $1.00\ m^*/m_0$, and increased with decreasing Se content and increasing I dopant content due to the increased carrier concentration.

Figure 3 shows the temperature dependence of the electrical conductivity of $Bi_{2-x}Sb_xTe_{3-y}Se_y:I_m$. The electrical conductivity can be expressed as [3]:

$$\sigma = ne\mu = \frac{ne^2\tau}{m^*} \quad (4)$$

where n is the carrier concentration, e is the electronic charge, μ is the carrier mobility, τ is the scattering time, and m^* is the carrier effective mass. The electrical conductivities of the specimens decreased with increasing temperature, showing behavior similar to degenerate semiconductors. As the Se content increased, the electrical conductivity decreased due to the decrease in carrier concentration. In addition, the $Bi_{1.9}Sb_{0.1}Te_{2.7}Se_{0.3}:I_{0.005}$ sample showed the highest electrical conductivity due to the increased carrier concentration caused by I doping. The electrical conductivity was largely unchanged with Sb substitution. The Sb occupation of the Bi site, as shown in Equation 3, was due to the donation of excess electrons due to

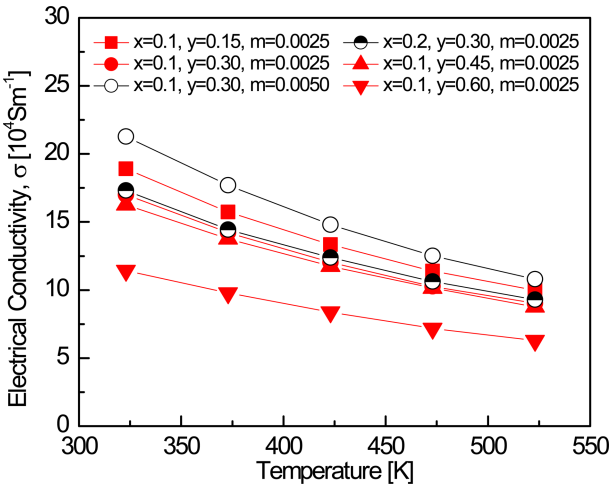

Fig. 3. Temperature dependence of the electrical conductivity of $Bi_{2-x}Sb_xTe_{3-y}Se_y:I_m$.

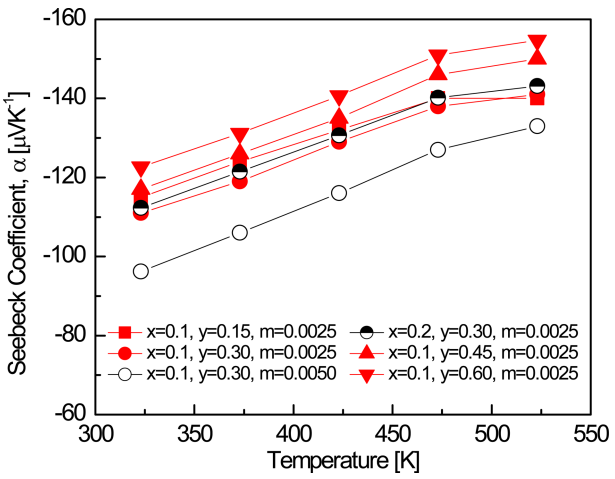

Fig. 4. Temperature dependence of the Seebeck coefficient of $Bi_{2-x}Sb_xTe_{3-y}Se_y:I_m$.

the formation of Te_{Bi} antisite defects; a similar phenomenon was also observed for Te_{Sb} antisite defects if the formation energies of these two antisite defects were identical.

Figure 4 shows the temperature dependence of the Seebeck coefficient of the $Bi_{2-x}Sb_xTe_{3-y}Se_y:I_m$ samples. All specimens exhibited negative Seebeck coefficients. The Seebeck coefficient (α) of the n-type semiconductor can be expressed as [19]:

$$\alpha = -(1+\lambda)\frac{8\pi^2 k_B^2 m^* T}{3eh^2}\left(\frac{\pi}{3n}\right)^{2/3} \quad (5)$$

where λ is the scattering parameter, k_B is the Boltzmann constant, and h is Planck's constant. The value of λ is zero when the carrier scattering is affected by the acoustic phonon mode. The absolute value of the Seebeck coefficient, |α| increased with increasing Se substitution due to the resulting decrease in carrier concentration. In addition, intrinsic transition occurs when the temperature is raised above a specific temperature. Thus, the Seebeck coefficient decreases with the peak value because the carrier concentration rapidly increases. The intrinsic transition temperature of quaternary Bi-Sb-Te-Se was higher than that of ternary Bi-Te-Se (473–523 K and 423 K, respectively) because the bandgap energy increases with increasing Sb content [20]. As shown in Equation 5, the Seebeck coefficient is proportional to the effective mass and inversely proportional to the carrier concentration. $Bi_{1.9}Sb_{0.1}Te_{2.85}Se_{0.15}:I_{0.0025}$, with the largest effective mass, would be expected to show the largest |α|; however, it was only |-115| μVK^{-1} at 323 K due to the high carrier concentration in the material. The maximum value of |α| was |-123| μVK^{-1} at 323 K for the $Bi_{1.9}Sb_{0.1}Te_{2.4}Se_{0.6}:I_{0.0025}$ sample.

Figure 5 shows the Pisarenko plots with different effective masses for the $Bi_{2-x}Sb_xTe_{3-y}Se_y:I_m$ samples. As shown in Table 1, $Bi_{1.9}Sb_{0.1}Te_{2.75}Se_{0.15}:I_{0.0025}$ and $Bi_{1.9}Sb_{0.1}Te_{2.7}Se_{0.3}:I_{0.005}$, with higher carrier concentrations, showed higher effective mass. Wang et al. [21] assumed that the potential barrier was influenced by band bending due to the dopant or substitution atoms leading to the energy filtering effect

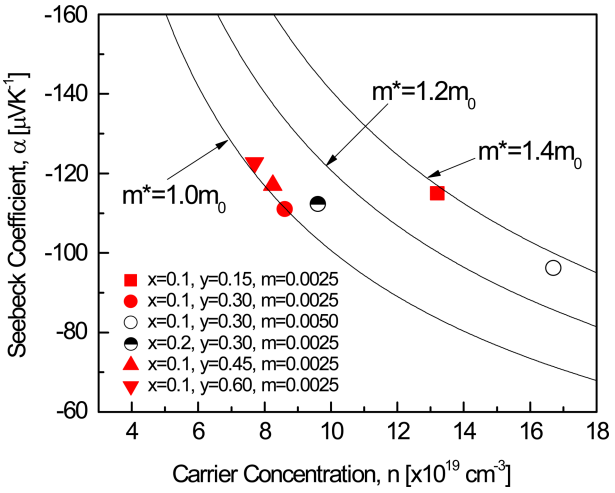

Fig. 5. Pisarenko plots with different effective masses for $Bi_{2-x}Sb_xTe_{3-y}Se_y:I_m$.

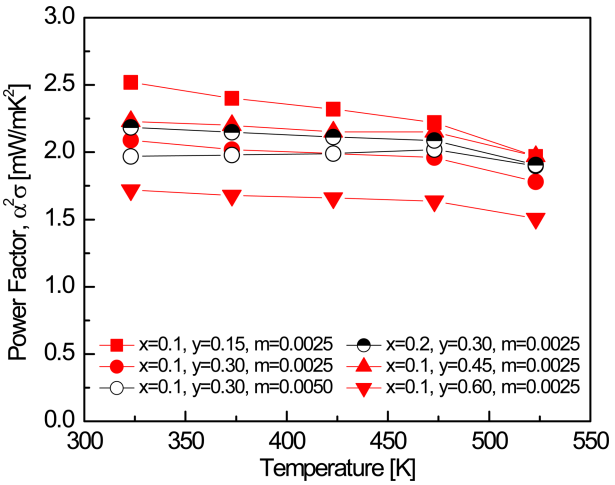

Fig. 6. Temperature dependence of the power factor of $Bi_{2-x}Sb_xTe_{3-y}Se_y:I_m$.

(the blocking of low-energy electrons through the transfer of high-energy electrons).

Figure 6 shows the temperature dependence of the power factor (PF) of the $Bi_{2-x}Sb_xTe_{3-y}Se_y:I_m$ samples. The PF can be expressed as [22]:

$$PF = \alpha^2\sigma \quad (6)$$

The PF can be enhanced by increasing the Seebeck coefficient and electrical conductivity. $Bi_{1.9}Sb_{0.1}Te_{2.4}Se_{0.6}:I_{0.0025}$ showed the highest Seebeck coefficient and the lowest electrical conductivity, resulting in the lowest PF value. $Bi_{1.9}Sb_{0.1}Te_{2.85}Se_{0.15}:I_{0.0025}$ showed the highest PF

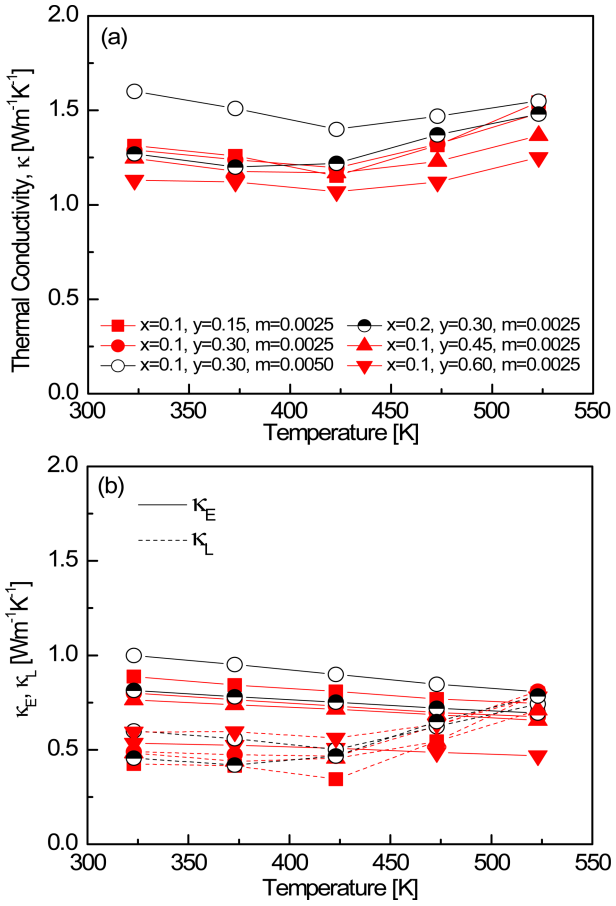

Fig. 7. Temperature dependence of the thermal conductivity of $Bi_{2-x}Sb_xTe_{3-y}Se_y:I_m$; (a) total thermal conductivity and (b) electronic and lattice thermal conductivities.

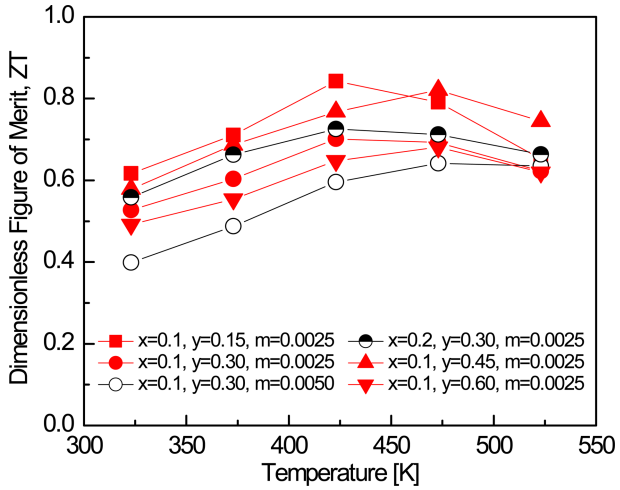

Fig. 8. Temperature dependence of the dimensionless figure of merit of $Bi_{2-x}Sb_xTe_{3-y}Se_y:I_m$.

of 2.52 $mWm^{-1}K^{-2}$ at 323 K due to its relatively high Seebeck coefficient and electrical conductivity, owing to its high effective mass and carrier concentration.

Figure 7 shows the temperature dependence of the thermal conductivity of the $Bi_{2-x}Sb_xTe_{3-y}Se_y:I_m$ samples. The thermal conductivity (κ) is composed of electronic thermal conductivity (κ_E) and lattice thermal conductivity (κ_L) components,

$$\kappa = \kappa_E + \kappa_L \quad (7)$$

which can be calculated using the Wiedemann-Franz law (L: Lorenz constant) [23], and $L = 2.0 \times 10^{-8}$ V^2K^{-2} was used in this study.

$$\kappa_E = L\sigma T \quad (8)$$

The thermal conductivity increased with increasing temperature due to bipolar conduction. The highest thermal conductivity of 1.6 $Wm^{-1}K^{-1}$ was obtained at 323 K for the $Bi_{1.9}Sb_{0.1}Te_{2.7}Se_{0.3}:I_{0.005}$ sample. The contribution of the electronic thermal conductivity was significant due to the increase in carrier concentration caused by I doping. In the I-doped specimens with m = 0.0025, the total thermal conductivity decreased due to the decrease in electronic thermal conductivity caused by Se substitution and the decrease in lattice thermal conductivity caused by the Sb substitution. The lowest thermal conductivity of 1.07 $Wm^{-1}K^{-1}$ (κ_L = 0.56 $Wm^{-1}K^{-1}$) was obtained at 423 K for the $Bi_{1.9}Sb_{0.1}Te_{2.4}Se_{0.6}:I_{0.0025}$ sample.

Figure 8 shows the dimensionless figure of merit (ZT) of $Bi_{2-x}Sb_xTe_{3-y}Se_y:I_m$. Eum et al. [24] reported a ZT of 0.89 at 423 K for n-type $Bi_{1.8}Sb_{0.2}Te_{2.7}Se_{0.3}$ prepared by encapsulated melting and hot pressing. Wang et al. [12] reported a ZT of 1.0 at 460 K for n-type $Bi_{1.9}Sb_{0.1}Te_{2.55}Se_{0.45}$ prepared by melt spinning and spark plasma sintering. In this study, n-type $Bi_{2-x}Sb_xT_{e3-y}Se_y:I_m$ was successfully synthesized using EM and HP processes. $Bi_{1.9}Sb_{0.1}Te_{2.85}Se_{0.15}:I_{0.0025}$ showed a similar thermal conductivity and higher PF compared with the other specimens, and had the highest ZT_{max} value of 0.84 at 423 K. As the extent of Sb and Se substitutions increased, the temperature of the ZT_{max} shifted higher due to the intrinsic transition and bipolar conduction.

4. CONCLUSIONS

Iodine-doped quaternary $Bi_{2-x}Sb_xTe_{3-y}Se_y:I_m$ solid solutions were prepared by EM and HP processes. All prepared specimens exhibited n-type characteristics. The lattice constants decreased with increasing Sb and Se substitution while they were largely unaffected by I doping. The Seebeck coefficient increased and the electrical conductivity decreased with increasing Se substitution. This was due to the decreased carrier concentration, which later increased with I doping. However, the charge transport properties were largely unchanged with differing levels of Sb substitution. The total thermal conductivity decreased due to the decrease in the electronic thermal conductivity caused by Se substitution and the decrease in the lattice thermal conductivity caused by Sb substitution. As a result, the highest PF of 2.52 $mWm^{-1}K^{-1}$ and the maximum ZT_{max} of 0.84 at 423 K were obtained for the $Bi_{1.9}Sb_{0.1}Te_{2.85}Se_{0.15}:I_{0.0025}$ specimen.

REFERENCES

1. J. F. Li, W. S. Liu, L. D. Zhao, and M. Zhou, *NPG Asia Mater.* **2**, 152 (2010).
2. L. E. Bell, *Science* **321**, 1457 (2008).
3. H. J. Goldsmid, *J. Appl. Phys.* **32**, 2198 (1961).
4. J. R. Drabble and C. H. L. Goodman, *J. Phys. Chem. Sol.* **5**,142 (1958).
5. L. V. Prokof'eva, D. A. Pshenai-Severin, P. P. Konstan-Tinov, and A. A. Shabaldin, *Semicond.* **43**, 1155 (2009).
6. S. H. Yoon, K. H. Lee, and S. J. Hong, *Kor. J. Met. Mater.* **55**, 123 (2015).
7. G. J. Snyder and E. S. Toberer, *Nat. Mater.* **7**, 105 (2008).
8. J. Seo, C. Lee, and K. Park, *J. Mater. Sci.* **35**, 1549 (2000).
9. M. Z. Tahar, S. A. Nemov, D. I. Popov, and T. E. Svechnikovad, *J. Phys.: Conf. Ser.* **150**, 022082 (2009).
10. H. P. Ha, Y. J. Oh, D. B. Hyun, and E. P. Yoon, *Intl. J. Soc. Mater. Eng. Resour.* **10**, 130 (2002).
11. X. A. Fan, J. Y. Yang, W. Zhu, S. Q. Bao, X. K. Duan, C. J. Xiao, and K. Li, *J. Phys. D: Appl. Phys.* **40**, 5727 (2007).
12. S. Y. Wang, W. J. Xie, H. Li, and X. F. Tang, *J. Phys. D: Appl. Phys.* **43**, 335404 (2010).
13. E. Clementi, D. L. Raimondi, and W. P. Reinhardt, *J. Chem. Phys.* **47**, 1300 (1967).
14. S. Y. Wang, W. J. Xie, H. Li, and X. F. Tang, *Intermet.* **19**, 1024 (2011).
15. H. Scherrer and S. Scherrer, *Thermoelectrics Handbook,* edited by D. M. Rowe, chap. 27, CRC Press, New York (2006).
16. T. S. Oh, D. B. Hyun, and N. V. Kolomoets, *Scr. Mater.* **42**, 849 (2000).
17. J. H. Son, M. W. Oh, B. S. Kim, S. D. Park, B. K. Min, M. H. Kim, and H. W. Lee, *J. Alloys Compd.* **566**, 168 (2013).
18. M. W. Oh, J. H. Son, B. S. Kim, S. D. Park, B. K. Min, and H. W. Lee, *J. Appl. Phys.* **115**, 133706 (2014).
19. K. Uemura and I. Nishida, *Thermoelectric Semiconductor and Their Application*, p.150, Nikkan-Kogyo Shinbun Press, Tokyo (1988).
20. B. Ryu, B. S. Kim, J. E. Lee, S. J. Joo, B. K. Min, H. W. Lee, S. Park, and M. W. Oh, *J. Kor. Phys. Soc.* **68**, 115 (2016).
21. S. Wang, H. Li, R. Lu, G. Zheng, and X. Tang, *Nanotechnol.* **24**, 285702 (2013).
22. L. Hu, H. Gao, X. Liu, H. Xie, J. Shen, T. Zhu, and X. Zhao, *J. Mater. Chem.* **22**, 16484 (2012).
23. H. Cailat, A. Borshchevsky, and J. P. Fleurial, *J. Appl. Phys.* **80**, 4442 (1996).
24. A. Y. Eum and I. H. Kim, *J. Kor. Phys. Soc.* **70**, 505 (2017).